Article ID: 1000-9116(2008)02-0118-09

Region-related features of crustal and upper-mantle velocity structure of the Chinese mainland detected by surface waveform modeling*

FENG Mei[1),♣] (冯 梅) AN Mei-jian[1)] (安美建) Suzan van der Lee[2)]

1) *Institute of Geomechanics*, *Chinese Academy of Geological Sciences*, *Beijing* 100081, *China*
2) *Department of Earth and Planetary Sciences*, *Northwestern University*, *Evanston IL* 60208-2150, *USA*

Abstract

Surface waveform modeling has played an important role on many continental-scale studies of upper mantle velocity structure, but it was seldom applied to the Chinese mainland study. The present study firstly analyzed surface waveform fittings for eight wave paths crossing through four different regions of the Chinese mainland (eastern, central, northern and western China), and then inverted for 1D path-averaged S-velocities for these paths. The inverted crustal and upper-mantle S-velocities showed obvious region-related features, which are well consistent with known geotectonic units and previous research results. These results indicate that surface waveform modeling is a reliable method to get crustal and upper-mantle velocity structure. Furthermore, this method has a prominent advantage in detecting upper-mantle structure compared with fundamental-mode surface-wave dispersion method.

Key words: **surface waveform modeling**; **region-related feature**; **crustal and upper-mantle S-velocity**; **Chinese mainland**

CLC number: P315.3^{+}1 **Document code**: A

Introduction

Compared with P wave, S wave phase is difficult to be recognized and contains large observational error. So, normally we seldom use S wave travel-time as direct observations to derive S-velocity structure but from surface-wave observations. There are two main methods to utilize surface wave to get S-velocity structure: one is using surface-wave group/phase velocity dispersions, the other is using surface waveforms. Because surface-wave dispersion processing is relatively easy and do not require focal mechanisms, while surface waveform synthesizing requires focal mechanism and strong computational effort, surface-wave dispersion methods have been widely used in studies on the crustal and upper mantle S-velocity structure of the Chinese mainland (FENG *et al*, 1981; Ritzwoller, Levshin, 1998; XU *et al*, 2000; Villaseñor *et al*, 2001; HE *et al*, 2002; ZHU *et al*, 2002; Huang *et al*, 2003), while studies using surface waveform meth-

* **Received** 2007-10-25; **accepted in revised form** 2008-01-21.
Foundation item: Natural Science Foundation of China (40504011, 40674058) and Basic Research Foundation of the Institute of Geomechanics, Chinese Academy of Geological Sciences (DZLXJK200707).
♣ **Author for correspondence**: mei_feng_cn@yahoo.com.cn

ods are very few (CAO *et al*, 2001; Lebedev, Nolet, 2003).

But the inefficiency of surface wave dispersion method is obvious. Because surface waveform is dominated mainly by fundamental-mode surface-wave energy, it is difficult to extract dispersions of higher-mode surface waves. That is why there are quite few surface-wave studies of the Chinese mainland using higher-mode dispersions. But higher-mode surface waves are more sensitive to deep Earth structure than fundamental-mode surface waves. So the current existed S-velocity models based on fundamental-mode dispersions have poor resolution in deep upper mantle (200~660 km). For instance, previous models for China and the eastern Asia based on fundamental-mode dispersions (Villaseñor *et al*, 2001) can hardly have resolution deeper than 200 km. Even for the model of ZHU *et al* (2002) who used long period surface waves (200 s), the resolution for depths deeper than 200 km is still very limited and is much poorer than depths above 200 km. On the other hand, surface waveforms contain both fundamental mode and higher mode surface waveform information which is more sensitive to deep structure. In the early of the 1990s, Nolet (1990) and Gee and Jordan (1992) started studying upper mantle by broadband seismic waveform modeling. Later, the partitioned waveform inversion method (PWI) proposed by Nolet (1990) have been widely applied to different regions of the world (Lebedev, Nolet, 1997, 2003; van der Lee, Nolet, 1997; Marone *et al*, 2004; Feng *et al*, 2007), however, only the study of Lebedev and Nolet (2003) covered part of China. CAO *et al* (2001) proposed a waveform inversion method similar to PWI and applied it to South China Sea area which is the first Chinese study on upper mantle using surface waveform modeling method. It is a pity that the PWI is not applied to study the whole Chinese (eastern Asia) mainland upper mantle while it has been successfully applied to the American and European continents. The present study is an attempt to apply PWI method to analyze waveform fittings and carry out 1D S-velocity inversions for several seismic ray-paths crossing through different regions of the Chinese mainland. And comparing inverted S-velocity models of different ray-paths, we show the reliability and importance of the PWI method in studies of crust and upper mantle structures.

1 Methodology

In the present study, surface waveform modeling is realized by the partitioned waveform inversion method (PWI), which was firstly developed by Nolet (1990), and later improved by van der Lee and Nolet (1997). For each seismic ray-path from event to station, we can construct the theoretical waveforms including Rayleigh and S waves by mode summation from fundamental mode up to the twentieth higher mode surface waves. Then by iteratively fitting the synthetic and observed waveforms, we can invert for 1D path-averaged crust and upper mantle velocity structure. In the present study, we use the global IASP91 model (Kennett, Engdahl, 1991) as initial model in theoretical waveform calculation. Iterative non-linear inversion method is used. Output model of previous iteration is taken as initial model for the next iteration till waveform misfit is small enough.

Figure 1 is an example of constructing synthetic waveform by mode summation of surface waves with given focal mechanism. The dashed line marks the theoretical S arrival. From top to bottom, the traces are respectively fundamental-mode surface waveform, synthetic waveform of the first two modes, synthetic waveform of the first three modes, and of the first twenty modes. From this figure, we can observe that fundamental mode surface wave only contains long-period waveform information, while with increase of mode branches, synthetic waveforms show more

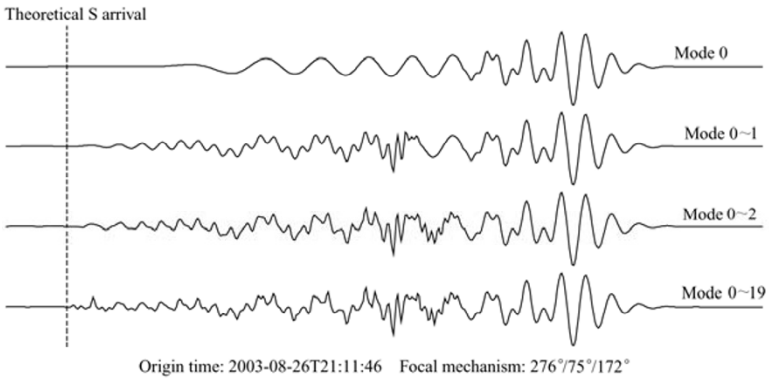

Figure 1 Illustration of constructing synthetic waveforms by mode summation with focal mechanism
The four traces are respectively fundamental model surface waveform (Mode 0), synthetic waveform of the first two modes (Mode 0~1), synthetic waveform of the first three modes (Mode 0~2) and the synthetic waveform of the first twenty modes (Mode 0~19)

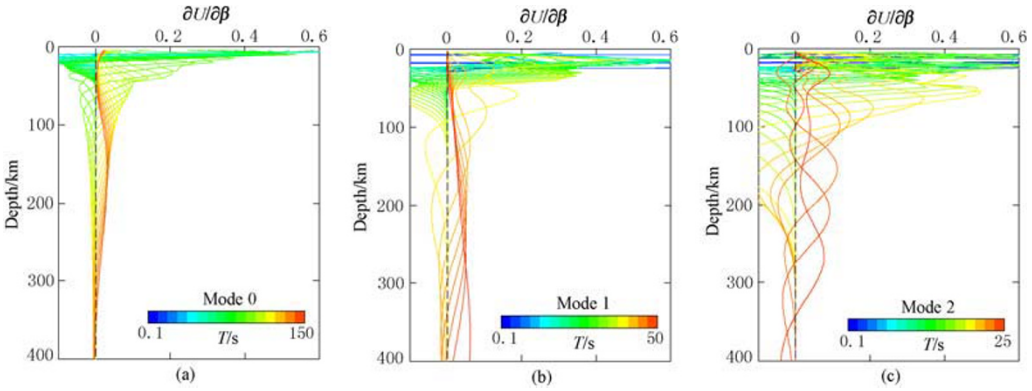

Figure 2 Sensitivity ($\partial U/\partial\beta$) of the fundamental-mode (a), first higher-mode (b) and second higher-mode (c) Rayleigh wave group velocity to S-velocity structure in different depth
For a same mode, the different colors represent sensitivities for different periods

detail. Especially when summation to the first twentieth mode, we can even reconstruct S wave very well. By inverting these surface waveforms synthesized with higher mode branches, we can obtain more reliable deep S velocity structure compared with only using fundamental mode surface waves. Figure 2 shows the partial derivatives ($\partial U/\partial\beta$) of surface-wave group velocity U to shear-wave velocity β at different depths. These derivatives can represent sensitivity (resolution) of surface waves to shear-wave velocities. A zero of $\partial U/\partial\beta$ means variation of shear-wave velocity structure will not cause variation of surface-wave (group-velocity). That is, surface-wave is insensitive to shear-wave velocity. While a nonzero of $\partial U/\partial\beta$ means variation of shear-wave velocity will cause variation of surface-wave, *i.e.*, surface-wave is sensitive to shear-wave velocity. So when $\partial U/\partial\beta$ is more different from 0, the surface-wave is more sensitive to shear-wave velocity. From Figure 2 one can see that for a same mode, long period surface wave is more sensitive to deep structures, while short period surface wave is more sensitive to shallow structure. Besides, Figure 2 also shows that the mode is higher, the surface wave is more sensitive to deep S velocity structure (sensitivity is more different from 0 where indicated by dashed line). So the present study use the mode summation method (sum to the first twenty modes) to construct the theoretical

Rayleigh and S waveforms, and then invert for crust and upper mantle velocity structure by iteratively fitting the synthetic and observed waveforms. A detail description of the PWI method is given in van der Lee and Nolet (1997).

2 Data and processing

As the objective of the present study is using waveform modeling method to detect the regional crust and upper mantle velocity structure of the Chinese mainland, here we selected waveform data for eight seismic ray-paths crossing through four different regions (eastern, central, northern and western) of the Chinese mainland, and each region was crossed by two seismic ray-paths. These waveform data are from two earthquakes with m_b>5.5 recorded by six CDSN permanent broad-band seismic stations. Table 1 lists the events source information and seismic stations recording the events. The event origin time and hypocentral information required by synthetic waveform are collected from the EHB catalogue (Engdahl *et al*, 1998), and the moment tensor (focal mechanism) are from the CMT catalogue (Dziewonski *et al*, 1983). In Table 1, we selected two earthquakes with different origin location, event depth and focal mechanism. And event *A* occurred in North China and its depth is shallow (13 km); while event *B* occurred around the border of the Afghanistan and Tajikistan on the west of China and its depth is relatively deep (175 km). The two events were respectively recorded by four seismic stations (last column of Table 1), forming eight seismic ray-paths crossing through four different regions of Chinese mainland. The waveform data of the eight ray-paths are the observation of the present study.

Table 1 Earthquake source and seismic station information

Event code	Date a-mo-d	Origin time (UTC) h:min:s	Epicentral location		Focal depth /km	m_b	Strike /°	Dip /°	Slip /°	Recording station
			λ_E/(°)	φ_N/(°)						
A	2004-03-24	01:53:48	118.28	45.38	13	5.6	167/352	28/62	86/92	MDJ, QIZ, KMI, LSA
B	2004-04-05	21:24:02	71.042	36.48	175	6.4	290/58	28/72	139/68	BJT, HIA, KMI, LSA

Ground displacement is normally extracted by deconvolving the observed waveforms with instrument response. But it is very important to note that waveform signals out of the stable instrument frequency band cannot be interpreted, so meanwhile deconvolving with instrument response, it is necessary to pre-process the waveforms with a band pass filter. The frequency range of the filter should be narrower than the instrument stable frequency band. Figure 3d is an observed waveform deconvolved by instrument response and pre-processed by a band-pass filter. As mentioned above, with mode summation method we can only synthesize S wave and surface wave, so after the pre-processing we still need to define a time-window to select the waveform segment that theoretically can be fit. Normally the time-window can start slightly earlier than S arrival and stop at the end of the surface wave tail (see Figure 3d). After cutting off the waveform inside the given time-window, another band-pass filtering is required to eliminate long period noise and diffraction signals. Here the frequency band should be much narrower than the stable frequency of the instrument, and for regional surface waves we selected 0.006~0.06 Hz (see Figure 3e). After processing all the observed waveforms with the above mentioned steps, then by iteratively fitting them with the synthetic waveforms, we can invert for the path-averaged velocity models for all source-to-receiver pairs.

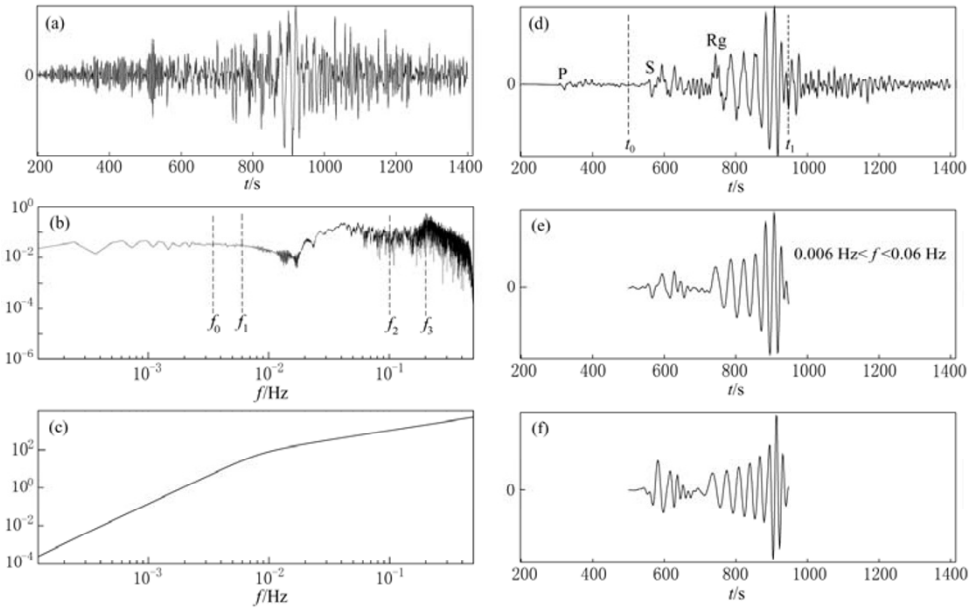

Figure 3 Waveform data processing steps

(a) Original observed waveform; (b) Observed waveform in frequency domain, where f_0 ~f_3 define the frequency band for pre-filtering; (c) Instrument response curve; (d) Observed waveform processed by band-pass filtering and deconvolved by instrument response, where t_0 and t_1 define the time-window of waveform (including S wave and surface wave) section to be fitted; (e) Observed waveform processed by further band-pass filtering and cut off by the time-window; (f) Synthetic waveform by mode summation

3 Results and discussion

Figure 4 gives the distribution of the eight ray-paths analyzed in the present study, and Figure 5 shows waveform fittings (left column) and their 1D velocity models (right column). Every two ray-paths in Figure 4 cross different regions of China, including the eastern, central, northern and western China. In the following we will give respective description and discussion on their waveform fitting and velocity model features.

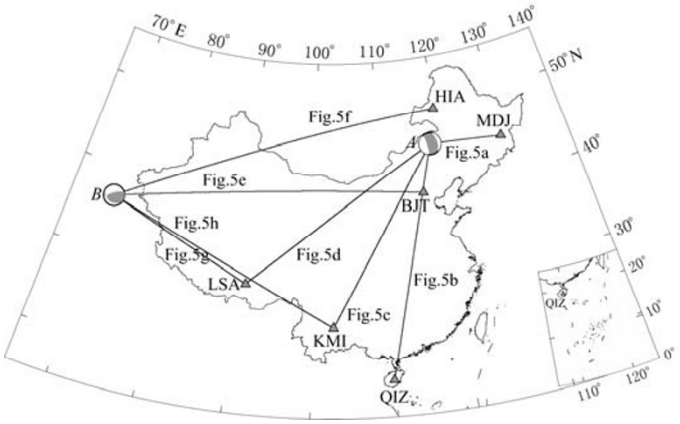

Figure 4 Distribution of eight ray-paths analyzed in the present study

3.1 Eastern China

Figures 5a and 5b show the waveform fittings and velocity profiles for two paths crossing through the eastern China (including Circum-Pacific tectonic domain). Figure 5a is for the ray from the shallow earthquake *A* to the station Mudanjiang (MDJ) and Figure 5b is for the ray from shallow earthquake *A* to the station Qiongzhou (QIZ). From these two sub-figures, we can see that the waveforms calculated from the IASP91 model can hardly fit the observed waveforms, while the waveforms calculated from the path-averaged model can fit the observed waveforms very well, which indicates that the path-averaged velocity model is more representative to the regional structure than the IASP91 model. Besides, the two paths crossing similar tectonic units show similar velocity structure. Generally, the crust in the Circum-Pacific region of the eastern China is thin (the Moho depth is shallower than 35 km of the global average model of IASP91). The crust velocity is similar to the IASP91 model, but the upper mantle above 200 km has lower velocity than the IASP91 model. Such structure features are consistent with the crust thickness model of Li *et al* (2006) and the velocity model of Huang *et al* (2003).

3.2 Central China

Figures 5c and 5d show the waveform fittings and velocity profiles for two paths crossing through the central China. Figure 5c is for the ray from the shallow earthquake *A* to the station Kunming (KMI) and Figure 5d is for the ray from shallow earthquake *A* to the station Lhasa (LSA). Again the synthetic waveforms calculated from the path-averaged model fit better the observed waveforms than the waveforms of the IASP91 model. Though both rays cross through the central Chinese mainland, the path from earthquake *A* to KMI mainly crosses the North China and the Yangtze platform and shows higher crust and lithosphere (100~200 km) velocity than the IASP91 model; while the path from earthquake *A* to LSA crosses a large part of the Qinghai-Tibetan Plateau and gives relatively low crust and lithosphere velocity. Both models show that the crust in central China is thicker than in eastern China. Paths crossing different tectonic units have quite different velocity structure, indicating that the central China is strongly lateral heterogeneous. This feature is well consistent with the crustal velocity model of FENG and AN (2007) and with the lithospheric velocity model of Huang *et al* (2003).

3.3 Northern China

Figures 5e and 5f show the waveform fittings and velocity profiles for two paths crossing through the northern China. Figure 5e is for the ray from the deep earthquake *B* to the station Beijing (BJT) and Figure 5f is for the ray from deep earthquake *B* to the station Hailar (HIA). Though both rays cross through several different tectonic units including the Paleo-Asian tectonic domain, previous studies showed that the lateral heterogeneity is weaker in the northern China than in the central China, and weaker in deep structure than in shallow structure. That is why the two different paths have similar upper mantle structure and weakly different lower-crust structure. In general, the northern China is characterized by thick crust, weak velocity perturbation in crust and upper mantle, and by homogeneous structure.

3.4 Western China

Figures 5g and 5h show the waveform fittings and velocity profiles for two ray paths crossing through the western China (including Tethyan tectonic domain). Figure 5g is for the ray from the deep earthquake *B* to the station LSA and Figure 5h is for the ray from deep earthquake *B* to the station KMI. Both rays have very similar paths and the two path-averaged velocity models show quite similar features. For example, the crustal and uppermost upper-mantle velocities are much lower than the IASP91 model, while the upper mantle velocity deeper than 150 km is higher than

IASP91. In general, the western China is characterized by thick crust thickness, low crustal and uppermost upper mantle velocity, and high upper mantle velocity in depths deeper than 150 km.

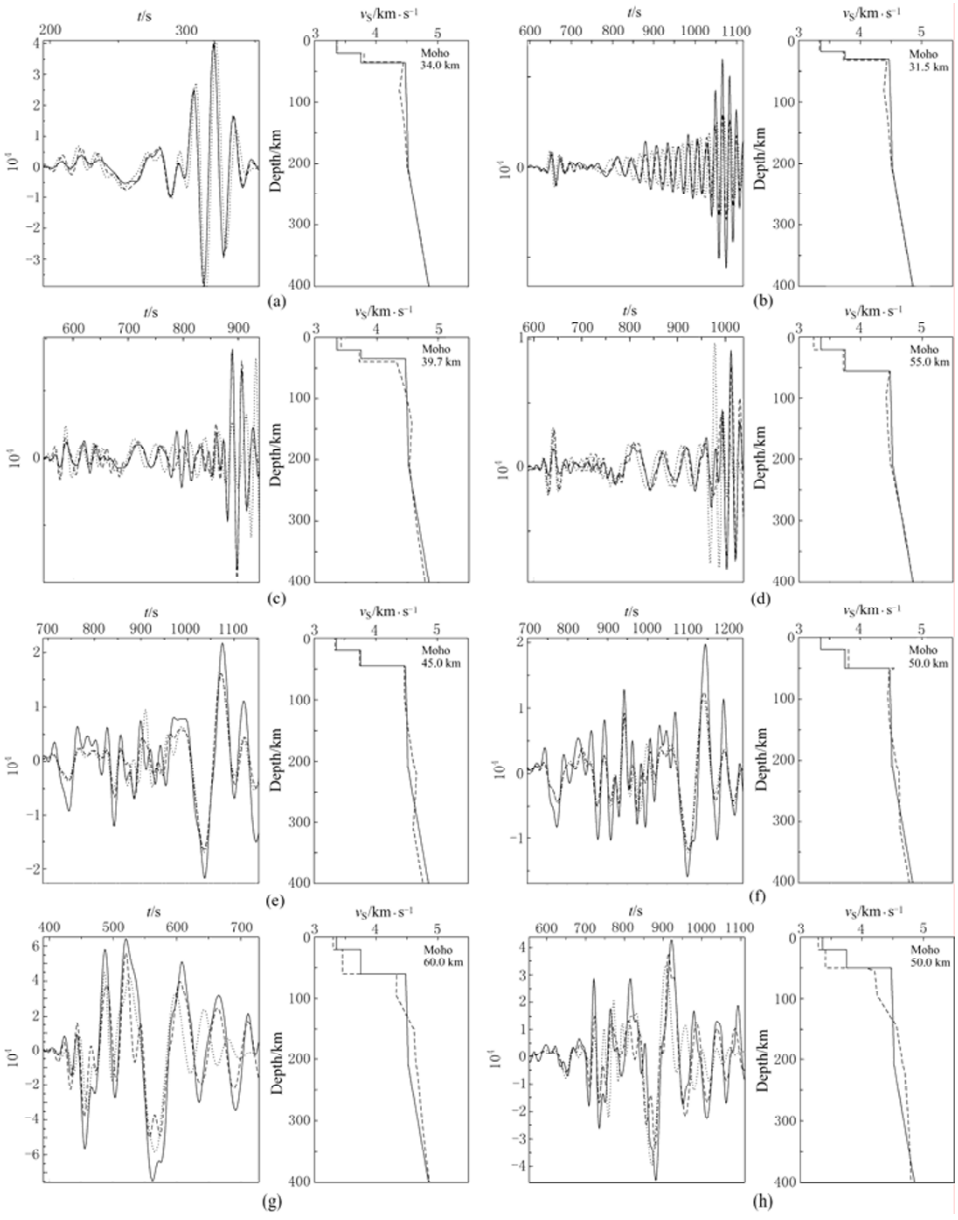

Figure 5 Waveform fittings (left column) and their 1D velocity models (right column) for the eight ray-paths analyzed in the present study. The two ray-paths crossed through the eastern China (a, b), through the central China (c, d), through the northern China (e, f), and through the western China (g, h)

On the left column, solid line denotes observed waveform, dotted line represents synthetic waveform from IASP91 model, dashed line is synthetic waveform from the path-averaged model and on the right column, solid line denotes IASP91 model, dashed line is the inverted path-averaged model and number in the top right corner is the path-averaged Moho depth

Compared the shallow earthquake *A* (Figures 5a~d) with the deep earthquake *B* (Figures 5e~5h), we can see the obvious difference in their waveforms. Firstly, surface waves propagate with higher speed in deep high-velocity media, so surface waves of deep earthquakes have less arrival-time difference with S waves. Secondly, waveforms of deep earthquakes take more information of deep earth structure which can be observed in the inverted velocity profiles. In Figure 5, the 1D velocity profiles inverted from waveforms of the deep earthquake *B* show stronger velocity perturbations in depths between 200 km and 400 km than the profiles of the shallow earthquake *A*.

According to the above waveform fitting analysis for different regions, different ray-paths crossing a same region can show similar or different velocity structures, which is mainly controlled by whether the ray paths cross through same tectonic units or whether the lateral heterogeneity is strong. The two velocity models for the central China are quite different from each other, while the two models for the eastern, northern and western China are very similar. Besides, models for different regions showed strongly region-related features. For example, the crust thickness is thin in eastern China, then increases in central and northern China, and is the thickest in the western China, which confirms that the crustal thickness of China is characterized by thin in east and thick in west. Compared with the other regions of China, the western China exhibits obvious low velocity anomaly in the crust and uppermost mantle. In summary, using surface waveforms as observations, synthetic waveforms can well fit observational waveforms by several iterations. And the inverted velocity models can represent the region-related features of the Chinese mainland velocity structure.

4 Conclusions

In the present study, we selected eight seismic ray-paths crossing through typical geotectonic units in different regions of the Chinese mainland (*e.g.*, Tethyan tectonic domain, Yangtze platform, North China platform, Paleo-Asian tectonic domain and Circum-Pacific tectonic domain, *etc*) and carried out surface waveform modeling analysis and velocity structure inversion for these ray-paths. The inverted results are well consistent with previous crustal-thickness and upper-mantle velocity models. Furthermore, the inverted velocity models for different regions show strongly region-related features, confirming that surface waveform modeling is a reliable method to study crustal and upper-mantle S-velocity structure. The other significance of the present study is that we analyzed and utilized the characteristic that higher-mode surface waveform has better sensitivity to deep structure than fundamental-mode dispersions. Then using surface waveform as observations, we inverted for velocity structure for a wider depths range including 200~400 km where traditional fundamental-mode dispersion inversion can hardly give reliable structures.

Acknowledgements We thank China Earthquake Data Center and DMC of IRIS for offering the seismic data. All figures are made with Generic Mapping Tool.

References

CAO Xiao-lin, ZHU Jie-shou, ZHAO Lian-feng, CAO Jia-min, HONG Xue-hai. 2001. Three dimensional shear wave velocity structure of crust and upper mantle in South China Sea and its adjacent regions by surface waveform inversion [J]. *Acta Seismologica Sinica*, **14**(2): 117-128.

Dziewonski A M, Friedman A, Giardini D, Woodhouse J H. 1983. Global seismicity of 1982: Centroid-moment tensor solutions for 308 earthquakes [J]. *Phys Earth Planet Interi*, **33**: 76-90.

Engdahl E R, van der Hilst R D, Buland R. 1998. Global teleseismic earthquake relocation with improved travel times and procedures for depth determination [J]. *Bull Seism Soc Amer*, **88**: 722-743.

FENG Mei and AN Mei-jian. 2007. Middle and upper crust shear-wave velocity structure of the Chinese mainland [J]. *Acta Seismologica*

Sinica, **20**(4): 359-369, doi:10.1029/2006JB004449.

Feng M, van der Lee S, Assumpcão M. 2007. Upper mantle structure of South America from joint inversion of waveforms and fundamental-mode group velocities of Rayleigh waves [J]. *J Geophys Res*, **112**: B04312, doi:10.1029/2006JB004449.

FENG Rui, ZHU Jie-shou, DING Yun-yu, CHEN Guo-ying, HE Zheng-qin, YANG Shu-bin, ZHOU Hai-nan, SUN Ke-zhong. 1981. Crustal structure in China from surface waves [J]. *Acta Seismologica Sinica*, **3**(4): 336-350 (in Chinese).

Gee L S, Jordan T H. 1992. Generalized seismological data functionals [J]. *Geophys J Int*, **111**(2): 363-390.

HE Zheng-qin, DING Zhi-feng, YE Tai-lan, SUN Wei-guo, ZHANG Nai-ling. 2002. Group velocity distribution of Rayleigh waves and crustal and upper mantle velocity structure of the Chinese mainland and its vicinity [J]. *Acta Seismologica Sinica*, **15**(3): 269-275.

Huang Z, Su W, Peng Y, Zheng Y, Li H. 2003. Rayleigh wave tomography of China and adjacent regions [J]. *J Geophys Res*, **108**(B2): 2 073, doi:10.1029/2001JB001696.

Kennett B L N, Engdahl E R. 1991. Traveltimes for global earthquake location and phase identification [J]. *Geophys J Int*, **105**: 429-465.

Lebedev S, Nolet G. 1997. The upper mantle beneath the Philippine Sea region from waveform inversions [J]. *Geophys Res Lett*, **24**(15): 1 051-1 854.

Lebedev S, Nolet G. 2003. Upper mantle beneath Southeast Asia from S velocity tomography [J]. *J Geophys Res*, **108**(B1): 2 048.

Li S L, Mooney W D, Fan J C. 2006. Crustal structure of mainland China from deep seismic sounding data [J]. *Tectonophysics*, **420**: 239-252.

Marone F, van der Meijde M, van der Lee S, Giardini D. 2004. Three-dimensional upper-mantle S-velocity model for the Eurasia-Africa plate boundary region [J]. *Geophys J Int*, **158**: 109-130.

Nolet G. 1990. Partitioned waveform inversion and two-dimensional structure under the Network of Autonomous Recording Seismographs [J]. *J Geophys Res*, **95**: 8 499-8 512.

Ritzwoller M H, Levshin A L. 1998. Eurasian surface wave tomography: Group velocities [J]. *J Geophys Res*, **103**(B3): 4 839-4 878.

van der Lee S, Nolet G. 1997. Upper-mantle S velocity structure of North America [J]. *J Geophys Res*, **102**: 22 815-22 838.

Villaseñor A, Ritzwoller M H, Levshin A L, Barmin M P, Engdahl E R, Spakman W, Trampert J. 2001. Shear velocity structure of central Eurasia from inversion of surface wave velocities [J]. *Phys Earth Planet Ints*, **123**: 169-184.

XU Guo-ming, LI Guang-pin, WANG Shan-en, CHEN Hong, ZHOU Hu-shun. 2000. The 3-D structure of shear waves in the crust and mantle of east continental China inverted by Rayleigh wave data [J]. *Chinese J Geophys*, **43**(3): 366-376 (in Chinese).

ZHU Jie-shou, CAO Jia-min, CAI Xue-lin, YAN Zhong-qiong, CAO Xiao-lin. 2002. High resolution surface wave tomography in East Asia and West Pacific marginal seas [J]. *Chinese J Geophys*, **45**(5): 679-698.